A Study of the Impact of Off-Equatorial Warm Pool SST Anomalies on ENSO Cycles

AMY SOLOMON

NOAA–CIRES Climate Diagnostics Center, Boulder, Colorado

FEI-FEI JIN

Meteorology Department, University of Hawaii at Manoa, Honolulu, Hawaii

(Manuscript received 28 April 2003, in final form 13 July 2004)

ABSTRACT

Concurrent with most large El Niño events, cold sea surface temperature (SST) anomalies are observed over the western Pacific warm pool region (WPWP). Observational evidence that SST anomalies that form in the off-equatorial western Pacific during El Niño–Southern Oscillation (ENSO) cycles are forced by subsurface ocean processes equatorward of 12°N and air–sea fluxes poleward of 12°N is presented. It is demonstrated that diurnal mixing in the ocean equatorward of 12°N plays a significant role in bringing subsurface temperature anomalies to the sea surface during an El Niño event.

The role of SST anomalies equatorward of 12°N in ENSO cycles is tested in the Zebiak–Cane coupled model, modified to allow for the impact of subsurface temperatures on SSTs. This coupled model successfully simulates cold SST anomalies in the off-equatorial northwestern Pacific that are observed to occur during the warm phase of ENSO and the atmospheric response to these anomalies, which is composed of both westerlies in the central Pacific and easterlies in the far western equatorial Pacific. It is found that there is little net change in the zonal mean wind stress at the equator, suggesting that the westerlies cancel the impact of the easterlies on the basin-scale tilt of the equatorial zonal mean thermocline depth. The anomalous westerly winds in the central equatorial Pacific are found to increase the amplitude of an El Niño event directly by increasing anomalous warm zonal advection and reducing upwelling. Moreover, the off-equatorial anticyclonic wind stress associated with the cold SST anomalies during the warm phase of ENSO tends to reduce the discharge of the equatorial heat content. Thus, the coupled processes over the western Pacific warm pool can serve as a positive feedback to amplify ENSO cycles.

1. Introduction

Classic theories of ENSO neglect ocean–atmosphere feedbacks in the western Pacific warm pool region (WPWP). These theories are motivated by the fact that SST anomalies during ENSO events are dominated by a pattern that covers the central to eastern equatorial Pacific. This is due to the so-called positive Bjerknes feedback, which operates in the central to eastern equatorial Pacific. Bjerknes (1969) was the first to recognize that tropical ocean–atmosphere interactions can amplify SST perturbations in the cold tongue region to sustain either a warm or a cold phase of ENSO. Anomalous easterly (westerly) trade winds force the thermocline depth, represented by a layer of sharp vertical temperature gradients that separates the upper ocean from the abyssal deep ocean, to be anomalously shallower (deeper) in the equatorial eastern Pacific than in the western Pacific. The trade winds also induce equatorial Ekman upwelling due to Coriolis effects, which effectively brings the cold water from the subsurface to the surface layer to enhance (reduce) the cold tongue in the eastern Pacific. At the same time, the atmospheric zonal pressure gradient caused by the east–west contrast of the cold (warm) SST anomaly drives an equatorial Walker circulation, which enhances (reduces) the surface easterlies over the Pacific basin and thus strengthens (weakens) the cold tongue, providing an explanation for the occurrence of the cold tongue and El Niño and La Niña events in the eastern equatorial Pacific.

The phase transition mechanism of ENSO has been largely attributed to dynamical ocean adjustment, which provides the needed delayed negative feedback to maintain ENSO oscillations. A number of conceptual models proposed to explain ENSO oscillations, such as the delayed oscillator (Suarez and Schopf 1988; Graham and White 1988; Battisti and Hirst 1989; Cane et al. 1990) and the recharge–discharge oscillator (Jin

Corresponding author address: Dr. Amy Solomon, NOAA–Climate Diagnostics Center, 325 Broadway, R/CDC1, Boulder, CO 80305-3328.
E-mail: Amy.Solomon@noaa.gov

1997), are all based on this assertion. These theories are supported by the success of intermediate coupled models in simulating interannual tropical Pacific variability without consideration of realistic ocean–atmosphere feedbacks in the WPWP or intraseasonal surface wind forcing. However, observational studies of the 1997–98 ENSO have shown that wind-forced upwelling Kelvin waves in the WPWP occurred at the peak of the El Niño event, suggesting that these waves may be playing a significant role in triggering the phase transition from an El Niño to a La Niña event (McPhaden and Yu 1999; Delcroix et al. 2000; Boulanger and Menkes 2001; Vialard et al. 2001; Picaut et al. 2002; Boulanger et al. 2003). These wind-forced Kelvin waves have been observed to occur during the 1986–89 and 1992–93 ENSO events as well (Delcroix et al. 1994; Boulanger and Menkes 1995).

Weisberg and Wang (1997) argue that easterly wind anomalies in the far western Pacific during the mature phase of an El Niño event are forced by changes in convective heating due to off-equatorial SST anomalies in the western Pacific. They assume that off-equatorial SST anomalies in the WPWP form due to variations in the depth of the thermocline in a region of mean upwelling, as is observed to occur in the equatorial eastern Pacific (Wang 2001). B. Wang et al. (1999) proposed that the cold off-equatorial SST anomalies that occur in the WPWP at the peak of an El Niño event are maintained through wind–evaporation feedbacks. Lau and Nath (2003) used a mixed layer ocean model coupled to an AGCM outside of the deep tropical equatorial Pacific to demonstrate that air–sea fluxes can create off-equatorial SST anomalies in the western Pacific similar to those observed to occur during ENSO events, providing support for the conslusions of B. Wang et al. (1999). However, the anomalies in the Lau and Nath study are much weaker than those observed to form during large ENSO events. Clearly, the relative importance of air–sea fluxes and ocean processes in creating these anomalies is still an open question. Both Weisberg and Wang (1997) and B. Wang et al. (1999) suggest that Kelvin waves triggered by these wind anomalies may be large enough to replace wave reflection as the delayed negative feedback that maintains ENSO oscillations. This feedback loop is referred to as the western Pacific oscillator (WPO).

The atmospheric response to off-equatorial WPWP SST anomalies was investigated by C. Wang et al. (1999) in an intermediate atmospheric model [it is interesting to note that in this study positions of the off-equatorial anomalies are at 10°N, where thermocline variations are observed to be large (B. Wang et al. 1999)]. This model study demonstrated that small SST anomalies in the off-equatorial WPWP are sufficient to produce equatorial easterly wind anomalies in the far western Pacific. The results of this study indicate that it is of interest to study the role of these anomalies in ENSO cycles independent of anomalies that form elsewhere, such as in the Indian Ocean. The C. Wang et al. (1999) study also found that the atmospheric response to these SST anomalies included equatorial westerly wind anomalies to the east of the SST anomalies. When these feedbacks were included in an intermediate coupled model, covarying eastern and western Pacific anomalies similar to observations were produced.

In this paper we reexamine how SSTs in the off-equatorial WPWP are formed and how they influence the evolution of an El Niño event. We use observational analyses to demonstrate that SST anomalies that form in the off-equatorial western Pacific during ENSO cycles are forced by subsurface ocean processes equatorward of 12°N and surface fluxes poleward of 12°N. We further show that SST anomalies in these regions peak at different times relative to equatorial eastern Pacific SST anomalies, suggesting that they play different roles in the ENSO cycle. Using subsurface data from the Tropical Atmosphere Ocean (TAO) Array, we illustrate the significance of diurnal mixing in creating the off-equatorial interannual SST anomalies. To investigate these feedbacks further we add oceanic mixing processes in the WPWP to the intermediate coupled model of the tropical Pacific developed by Zebiak and Cane (1987). These intermediate model studies provide evidence that the net effect of the off-equatorial SST anomalies equatorward of 12°N is to amplify El Niño events.

2. Surface heat balance in the WPWP

It has been noted by Harrison (1996), Weisberg and Wang (1997), and B. Wang et al. (1999) that associated with most large El Niño events, there are observed to be cold SST anomalies over the WPWP. For example, Fig. 1 shows the spatial structure of SST and wind stress anomalies at the peak of the two largest El Niños since 1980. These El Niños are seen to have large SST anomalies in both the Niño-3.4 (5°S–5°N, 170°–120°W) and Niño-6 (8°–16°N, 140°–160°E) regions. During the 1982 and 1998 El Niños anticyclonic wind stress anomalies in the northwestern WPWP are seen to occur in the region of the off-equatorial SST anomalies. These anticyclonic wind stress anomalies have an easterly component on the equator in the Niño-5 region (5°S–5°N, 120°–140°E). The Niño-5 and Niño-6 indices are defined following the study of C. Wang et al. (1999). Similar SST and wind stress anomalies have been observed during other major El Niño events (B. Wang et al. 1999). Of particular interest to this study is that the SST anomalies in the WPWP during the peak phase of these large El Niño events tend to occur *equatorward* of 12°N, that is, equatorward of the WPWP anomalies seen in composites of El Niño events (Rasmussen and Carpenter 1982; C. Wang et al. 1999; among others). For this reason we define two new indices, Niño-6N

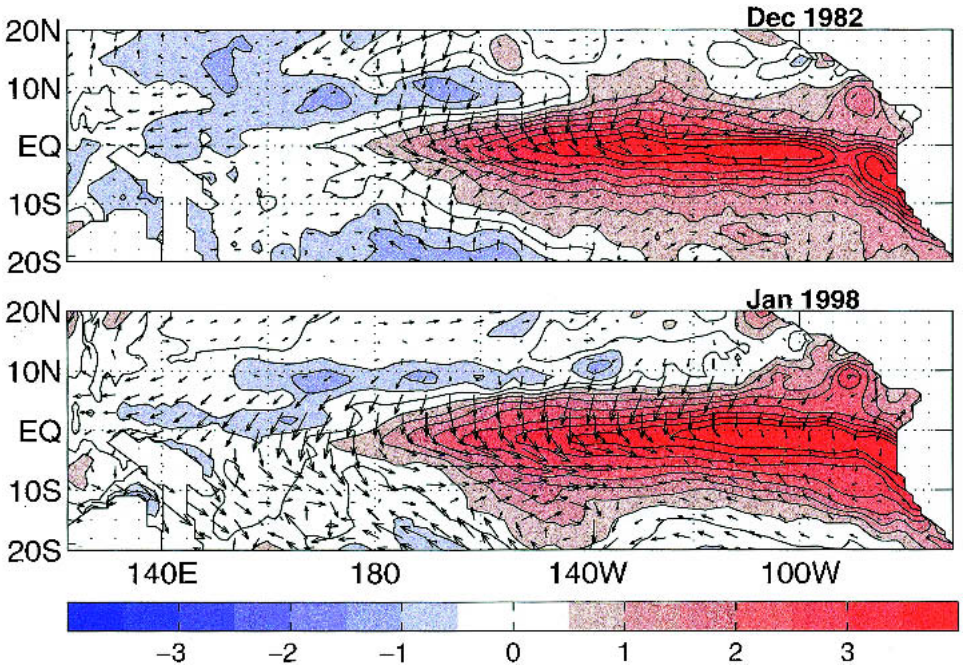

FIG. 1. Spatial structure of SST and wind stress anomalies for the two largest El Niños since 1980: (a) Dec 1982 and (b) Jan 1998. SST anomalies are shown with a contour interval of 0.5°C. Wind stress anomalies shown with vectors in units of N m^{-2}.

(12°–16°N, 140°–160°E) and Niño-6S (5°–9°N, 140°–160°E).

Figure 2 shows the Niño-3.4, Niño-6N, and Niño-6S indices from 1997 to 1999. These indices were calculated using monthly mean averages of SST anomalies from the National Oceanic and Atmospheric Administration Pacific hindcast. In this hindcast, observed surface and subsurface ocean temperatures as well as satellite altimetry sea level data from TOPEX/Poseidon are assimilated into a Pacific basin ocean general circulation model (Behringer et al. 1998). The model is forced with weekly mean National Centers for Environmental Prediction (NCEP) operational atmospheric analyses of surface winds and heat fluxes. During the onset to peak phases, following the definitions of ENSO phases from Rasmussen and Carpenter (1982), of the El Niño and La Niña events anomalies in the Niño-6S region are larger than anomalies in the Niño-6N region. In addition, anomalies in the Niño-6N region tend to peak after anomalies in the Niño-3.4 region have decayed away. These results suggest that different processes are forcing anomalies in the Niño-6N and Niño-6S regions.

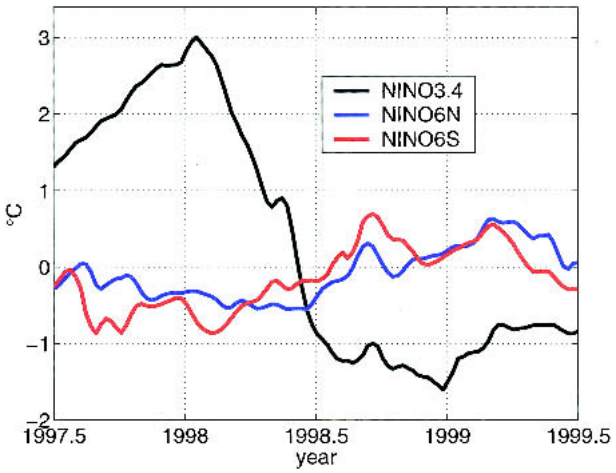

FIG. 2. Time series of Niño-3.4 (5°S–5°N, 170°–120°W), Niño-6N (12°–16°N, 140°–160°E), and Niño-6S (5°–9°N, 140°–160°E) indices from Jul 1997 to Jul 1999 using SST anomalies from the NOAA Pacific hindcast, in °C. All indices smoothed with a 3-month running mean filter.

In order to assess whether different processes are responsible for creating SST anomalies in the Niño-6N and Niño-6S regions, surface heat budgets were calculated using weekly averaged data from the NOAA Pacific hindcast. The heat budget was calculated following the fixed thickness method of Feng et al. (1998), where the bottom of the surface layer was set to 50 m. Instead of calculating the vertical advection term, we chose to estimate vertical mixing as the residual of the heat budget, following Cronin and McPhaden (1997). Therefore, the residual of the surface heat budget is composed of vertical advection, vertical turbulent fluxes, and estimation errors. To identify the contributions of these SST tendencies to the SST anomalies, we integrate them

with respect to time starting around the middle of 1997 when the SST anomalies are nearly zero in these regions.

Figure 3 shows the cumulative contributions of horizontal advection, fluxes, heat storage, and the residual to the SST anomaly budget in the Niño-6N region from June 1997 to June 1998. The storage term when integrated is by definition the SST anomaly itself. It is seen that in this region, the SST anomaly is of the same sign as the contribution from surface fluxes, whereas the contribution from the residual tends to oppose the SST anomaly. In other words, surface fluxes tend to force the anomalies, while three-dimensional subsurface processes tend to damp them. In addition, during periods when the storage term is large, advection is a forcing term (this was determined from tendency terms not shown).

Figure 4 shows the cumulative contributions of horizontal advection, fluxes, heat storage, and the residual to the SST anomaly budget in the Niño-6S region from June 1997 to June 1998. From June 1997 until September 1997, the contributions from fluxes and the residual force the surface heat anomalies. From September 1997 until June 1998, the residual is a forcing term and the fluxes damp the surface heat anomalies. Also, different from the SST anomaly balance in the Niño-6N region, when the storage term is large, the advection term is small in this region (this was determined from tendency terms not shown). Therefore, during the peak phase of the El Niño event it appears that the subsurface three-dimensional processes are responsible for the cold SST anomalies in this region. In the next section we will demonstrate that these anomalies form, in part, due to the mixing of cold thermocline water into the surface layer by diurnal mixing.

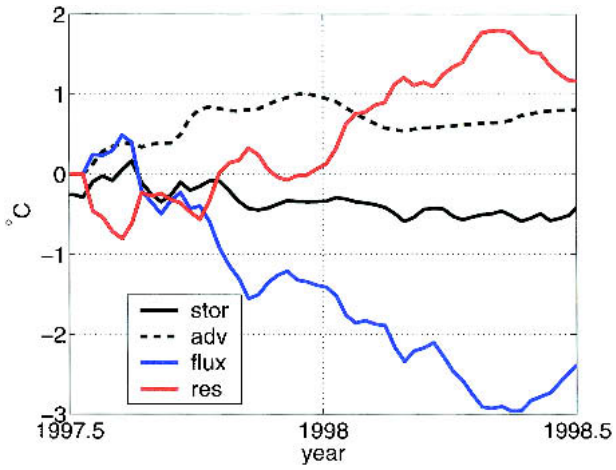

FIG. 3. Cumulative surface layer temperature tendency from 0 to 30 m in the Niño-6N region calculated with weekly NOAA Pacific hindcast data from June 1997 to June 1998. The advection term includes both zonal and meridional advection. The residual term includes vertical advection, vertical turbulent fluxes, and estimation errors. The flux term includes penetrative radiation and surface fluxes. All terms are shown in °C.

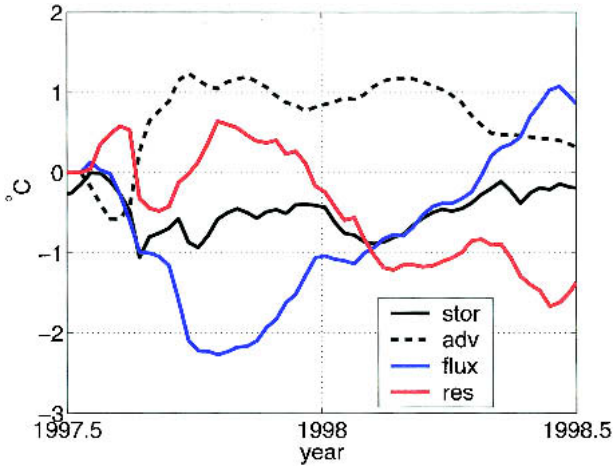

FIG. 4. As in Fig. 3 but for the Niño-6S region.

3. Linkage of SST and Z_{20} anomalies in the WPWP

a. Correlations between SST and Z_{20} anomalies in the WPWP

In the previous section we have shown that subsurface processes contribute to forcing the cold SST anomalies in the Niño-6S region at the peak of an El Niño event. Given that the thermocline is relatively deep and climatological upwelling is weak (Helber and Weisberg 2001) in the western Pacific, what processes cause the surface to be sensitive to variations in the thermocline depth? In order to answer this question we calculated the correlation between September mean SST and 20°C isotherm depth (Z_{20}) anomalies from 1950–2000 using the Simple Ocean Data Assimilation (SODA) ocean temperatures (Fig. 5). SODA is provided by the University of Maryland (Carton et al. 2000a,b). This data assimilation uses a forecast model based on Geophysical Fluid Dynamics Laboratory (GFDL) ocean physics driven by historical meteorology (winds, heating, rainfall − evaporation), assimilating historical observations of temperature salinity, sea level, SST, and surface current. The deep thermocline in the western Pacific and shallow thermocline in the east Pacific can be clearly seen. Of particular interest to this study is the relatively shallow thermocline in the northwest WPWP. Surface wind stress curl in the intertropical convergence zone (ITCZ) brings the thermocline closer to the surface between 4°N and 11°N. The thermocline depth in this region is shallowest in September when the annual Rossby wave amplitudes peak in the western Pacific (Wang et al. 2000). Although the off-equatorial thermocline in the northwest WPWP is deep relative to the eastern tropical Pacific, there is significant correlation between the SST and Z_{20} anomalies between 4° and 10°N, 130° and 150°E. A small region of significant correlations in the South Pacific along the western boundary is also observed.

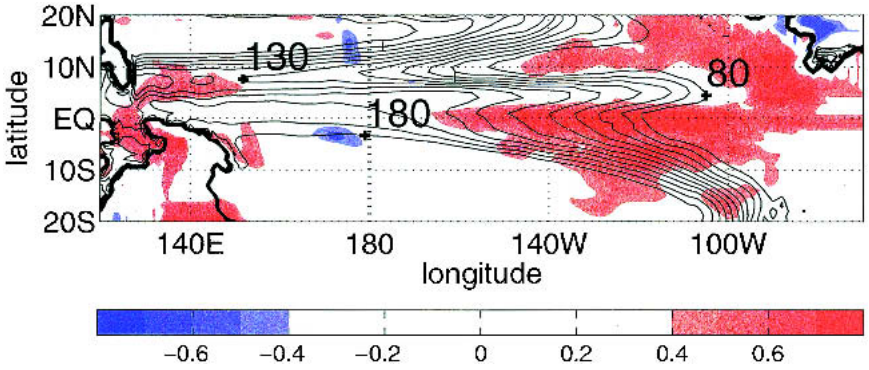

FIG. 5. Sep monthly mean Z_{20}, in m, shown with contours. Correlation between SST and Z_{20} anomalies are shown with shading. Only greater than 99% significant correlations are shaded. This figure was generated using Sep 1950–2000 SODA data assimilations products.

Figure 6 plots the correlation between Z_{20} and ocean temperature for depths up to 100 m using monthly mean SODA data from 1950 to 2000 for the TAO Array (Mangum et al. 1998) buoy locations at (a) 5° and (b) 8°N. The dashed lines in the figure show the 99% significance levels. Figure 6a shows that Z_{20} is significantly correlated with ocean temperature from 100 m to the surface at 137° and 147°E. Correlations at 156° and 165°E are also highly correlated, although not significant to 99%, considering that all months in the time series are used in the correlation and not just September. Large correlations from 100 m to the surface are also seen at 8°N (Fig. 6b). Since the shallow thermocline in the northwest WPWP is absent in the South Pacific (Fig. 5), the correlations are lower south of the equator (results not shown).

b. The role of diurnal mixing

Figure 7 shows the monthly mean ocean temperatures in the Niño-6S region for the 1982/83 (Fig. 7a) and 1997/98 (Fig. 7b) ENSO events. These ocean temperatures were taken from the NOAA Pacific hindcast. Cold SST anomalies of the order of 1°C are observed during the peak phase of both El Niños. The thermocline depth is indicated by masking all temperatures below 25°C, which we will refer to as Z_{25}, a more meaningful indicator of the thermocline depth in this region of the WPWP than Z_{20}. The thick black line in both figures indicates the climatological monthly mean Z_{25} for the 1980–2002 dataset. Comparing Z_{25} during each period with the climatological mean Z_{25}, it is seen that the anomalously cold SSTs are associated with Z_{25} coming up to within 60 m of the surface. An anomalously deep thermocline is also observed during the onset of the La Niña events.

However, what causes the surface to be sensitive to these variations in thermocline depth in a region where upwelling is observed to be weak? To answer this question we calculated the 30-day running mean variance of 2-day high-pass-filtered hourly TAO ocean tempera-

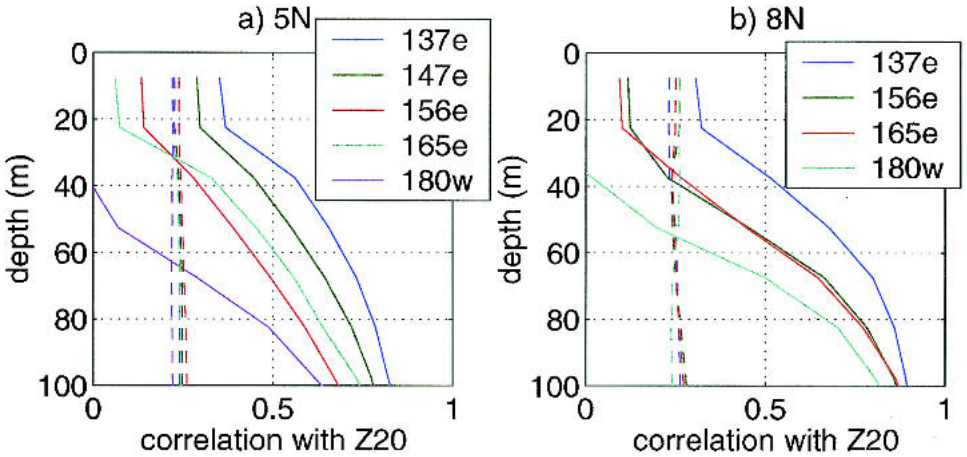

FIG. 6. Correlation between Z_{20} and ocean temperature for depths up to 100 m using monthly mean SODA data from 1950–2000 for TAO buoy locations at (a) 5°N and (b) 8°N. The dashed lines show the 99% significance levels.

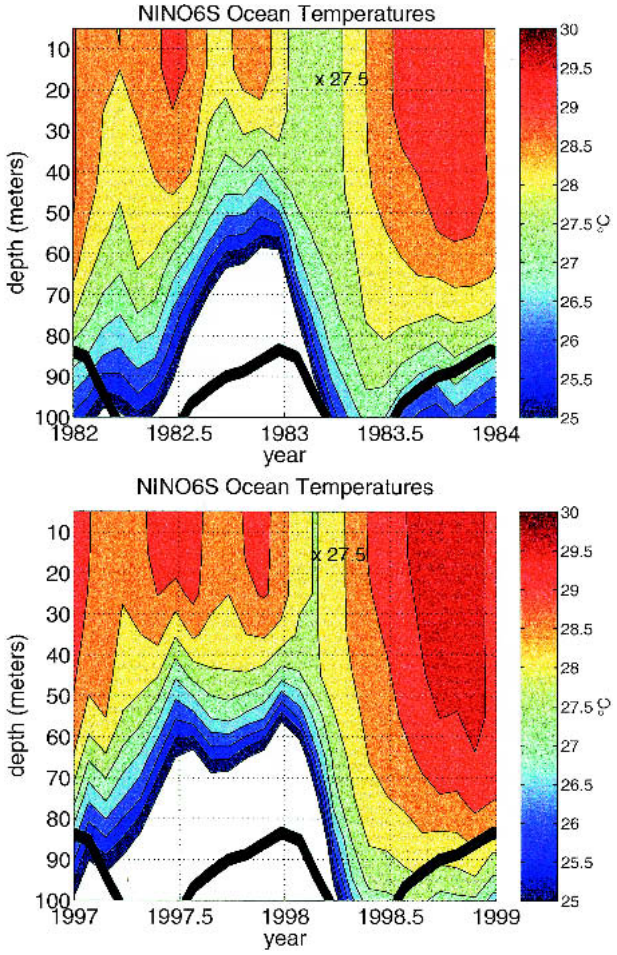

FIG. 7. Niño-6S ocean temperatures for depths to 100 m using monthly mean NOAA Pacific hindcast, in °C. Temperatures less than 25°C are masked out to highlight the Z_{25} contour. The thick black line indicates the climatological monthly mean Z_{25}. (a) 1982–83. (b) 1997–98.

tures at 5°N, 165°E and 50–100 m. Ocean temperatures at this location were used in the analysis since this was the closest TAO buoy to the Niño-6S region with hourly data available during 1997/98. A minimum depth of 50 m was chosen based on the minimum depth of the thermocline in Fig. 7b. Figure 8 plots the standard deviation of the 30-day running mean variance at 50, 75, and 100 m. The data are plotted for the 1997/98 ENSO event. Large variance is seen during the onset and peak phases of the El Niño event at 50 m. The peak in variance occurs at deeper levels as the El Niño evolves, deepening from 50 to 100 m at the beginning of 1998. At least 40% of the total variance during the onset and peak phases of the El Niño event is explained by variability on time scales shorter than 2 days. Moreover, the majority (about 80%) of the variance in the high frequency variability comes from the period window from 0.5 to 2 days (results not shown). This is a clear indication that diurnal mixing can more efficiently mix cold water from the thermocline into the surface layer when the thermocline comes within 60 m of the surface. This is a nonlinear process since this is not observed during the La Niña event. Together, Figs. 4, 7, and 8 suggest that subsurface three-dimensional processes are the dominant forcing of cold SST anomalies in the Niño-6S region during the onset and peak phases of the two largest El Niños since 1980.

4. Intermediate coupled model runs

The results of C. Wang et al. (1999) demonstrate that cold SST anomalies in the Niño-6 region, observed to occur during the peak phase of an anomalously large El Niño event, can force surface wind anomalies composed of both equatorial easterlies in the WPWP and westerlies in the central Pacific. The question that will be addressed in this section is what role do these cold SST anomalies in the western Pacific region play in ENSO cycles? This question is explored with the use of the Zebiak and Cane (1987) intermediate coupled model of the Pacific basin (hereafter referred to as the ZC model) with four added modifications.

First, the mean thermocline depth in the northwest WPWP is decreased from 165 to 120 m to simulate the observed relatively shallow thermocline depth in the northern WPWP. Second, since the subsurface temperature is unrealistically insensitive to thermocline depth variations in the WPWP in the ZC model, the b_2 parameter is decreased from 3.0 to 1.2 in the northern WPWP. Parameterizing the relatively shallow thermocline in the WPWP with these two modifications was first proposed by C. Wang et al. (1999).

In addition, we add a third modification by adding a term to the SST tendency equation to represent diurnal mixing. We assume that diurnal mixing can be param-

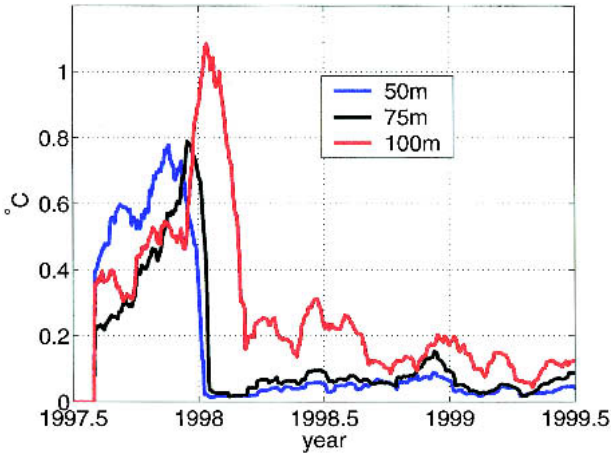

FIG. 8. Standard deviation of 30-day running mean variance of 2-day high-pass hourly TAO ocean temperatures at 5°N, 165°E and 50 m (blue), 75 m (black), and 100 m (red), in °C.

eterized as a diffusive mixing of the subsurface water into the mixed layer between 5° and 9°N. This additional SST tendency term can be written as

$$T_t = -(T_1 - T_{\text{sub}})\alpha_d^{-1},$$

where T_1 is the SST anomaly, T_{sub} is the subsurface temperature anomaly, and α_d is the diffusion time scale, which is varied from 150 to 300 days. Furthermore, we include a nonessential modification by setting the minimum wind speed in the WPWP to 5 m s^{-1}. A 1000-yr integration adding only this modification to the ZC model is indistinguishable from the control integration using standard ZC parameters. This change has little impact in the standard ZC model because in this version of the ZC model the heat flux feedback is independent of wind speed.

a. Coupled model runs

Three runs with the coupled model will be discussed. The control run (referred to as CNTL) uses the standard parameters of the ZC model without any additional feedbacks. Details of this model setup are provided in Zebiak and Cane (1987). The second run (referred to as PERT1) includes all of the additional processes with a diffusion time scale of 200 day^{-1}. The third run (referred to as PERT2) is the same as the second run except that the thermal restoring time scale in the surface heat flux is increased (tloss = 0.975) to eliminate interannual oscillations when the control setup is used.

Figure 9 shows that adding the additional feedbacks in the WPWP causes the ENSO events in PERT1 to occur more regularly than in CNTL. This figure also shows that the maximum amplitude of ENSO events in these two runs is very similar. However, it is seen that the PERT1 has many more events close to this peak value. This is evidence that these feedbacks in the WPWP act to increase the amplitude of ENSO events and also tend to prolong the period by about 6 months.

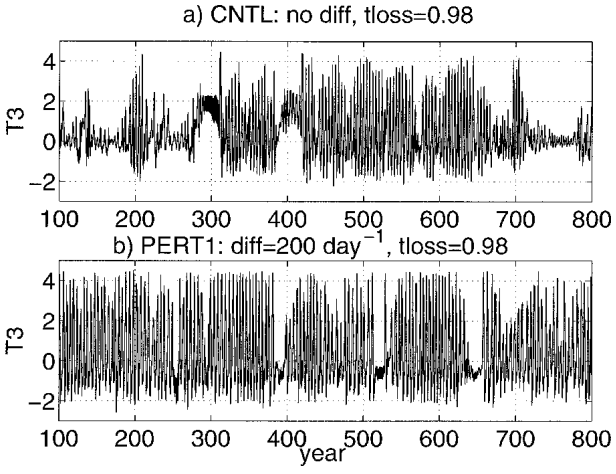

FIG. 9. 700-yr time series of SST anomalies in the Niño-3.4 region using the ZC model, in °C: (a) CNTL, (b) PERT1.

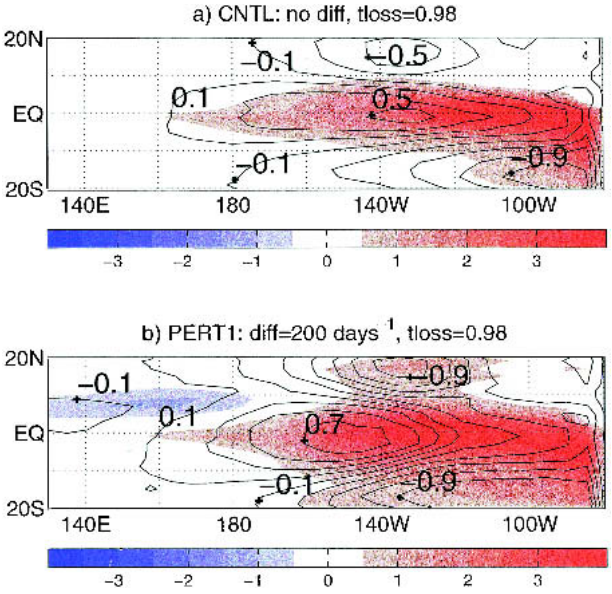

FIG. 10. Spatial structure of SST and wind stress anomalies at the peak of an El Niño event for the (a) CNTL and (b) PERT1, using the ZC model: SST anomalies shown with a contour interval of 0.5°C; wind stress anomalies shown with vectors in N m^{-2}.

Figure 10 shows anomalous zonal wind stress and SST at the peak of an El Niño event from the CNTL and PERT1 runs. The El Niños were chosen to have comparable magnitudes. The El Niño from CNTL shows no SST or wind stress variability in the WPWP. By contrast, The El Niño from PERT1 shows SST and wind stress close to those observed (Fig. 1).

Figure 11 shows a 300-yr time series of SST anomalies in the Niño-3.4 region (T3) for the PERT2. This is the model setup that does not support interannual variability when the feedbacks in the WPWP are neglected. This time series shows that adding the feedbacks in the WPWP causes the model to oscillate with a 4-yr period. This is an indication that the ENSO mode of the model has changed from a subcritical to a supercritical regime. In other words, there is an increase in the growth rate of the ENSO mode. This confirms that the additional feedbacks in the WPWP act as a positive feedback for ENSO events.

b. Atmosphere-alone model runs

In order to explore these results more fully, a series of runs were done with the uncoupled atmospheric component of the ZC model. First, an additional coupled model run (referred to as PERT3) was done that applied the additional WPWP feedbacks between 1° and 5°N so that the atmospheric response at the

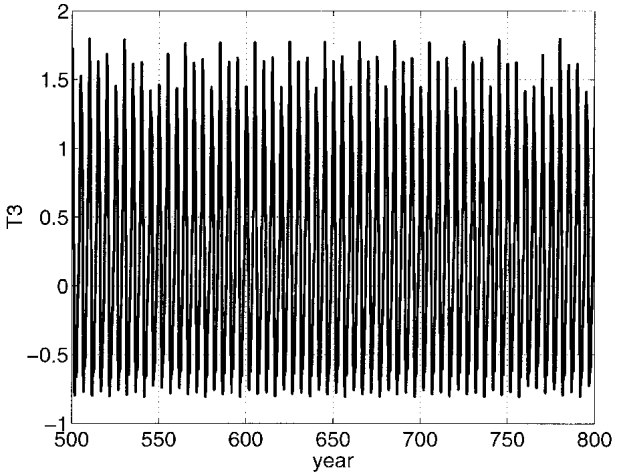

FIG. 11. 300-yr time series of PERT2 SST anomalies in the Niño-3.4 region, in °C.

equator is enhanced. Then two runs were done using only the atmospheric part of the ZC model. This atmospheric model was forced with SST anomalies at the peak of an El Niño event from PERT1 and PERT3. The results of these runs are plotted in Fig. 12. The top two plots (Figs. 12a,b) are from the PERT1, where Fig. 12a shows the SST anomalies at the peak of an El Niño event and Fig. 12b displays the difference between the zonal wind stress from runs with and without the SST anomalies in the WPWP region (with minus without). The SST anomalies without the WPWP SST anomalies look exactly the same as Fig. 12a except that all negative SST anomalies west of 160°W are set to zero. Figures 12c,d are exactly the same as Figs. 12a,b except that the additional WPWP feedbacks are applied between 1°N and 5°N instead of 5° and 9°N.

The atmospheric response to the SST anomalies in the WPWP is consistent with the atmospheric response to off-equatorial SST anomalies, as demonstrated by C. Wang et al. (1999). In other words, the cold SST anomalies in the WPWP region produce a Gill-type asymmetric response. For both sets of runs the change in the zonal mean zonal wind stress between 3°S and 3°N is essentially zero (less than 0.02 N m^{-2}). In addition, in this atmospheric response there is a strong anticyclonic wind stress curl in the western Pacific.

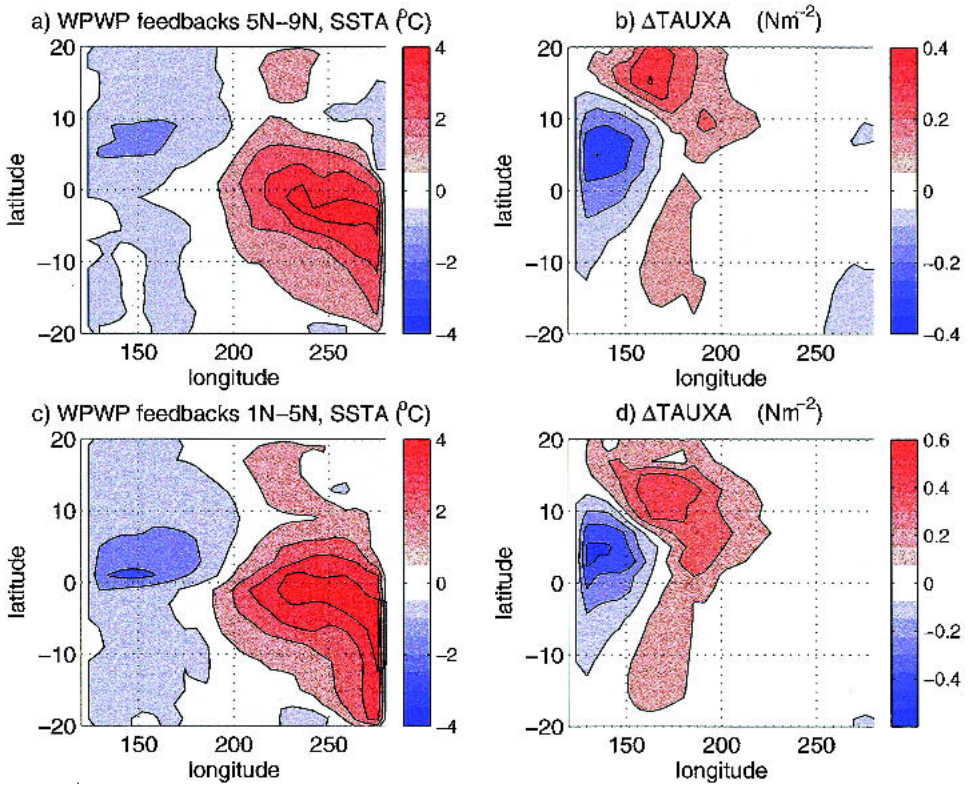

FIG. 12. Results from the stand-alone ZC atmospheric model runs: Model setup described in the text. (a) SST anomalies at the peak of an El Niño event from PERT1, in °C. (b) Zonal wind stress difference between runs forced by PERT1 SST anomalies at the peak of an El Niño event with and without WPWP SST anomalies (with − without), in Nm^{-2}. (c) SST anomalies at the peak of an El Niño event from PERT3, in °C. (d) Zonal wind stress difference between runs forced by PERT3 SST anomalies at the peak of an El Niño event with and without WPWP SST anomalies (with − without), in N m^{-2}.

c. *Ocean-alone model runs*

Clearly, the atmosphere-alone runs show that the atmospheric response to the cold SST anomalies in the WPWP have the potential of amplifying an El Niño event. To understand how these anomalous winds impact ocean variability, a series of model runs was done with the ZC ocean component alone. In these model runs the ocean model is forced with four different wind patterns, all modulated on a 4-yr time scale. The wind patterns were taken at the peak of an El Niño event from PERT1 and PERT3 with and without cold SST anomalies in the WPWP. Figure 13a shows the zonal wind stress response to the PERT1 cold SST anomalies alone in the WPWP at the peak of an El Niño event. Figure 13b shows the ZC ocean model's response to this wind forcing. These results clearly show that the atmospheric response to the cold SST anomalies alone can trigger an El Niño. To isolate the ocean's response to the anomalous easterlies, we forced the ocean model with only the easterly wind stress anomalies in the WPWP. The ocean model's response to this wind forcing is a slight cooling in the equatorial Pacific between 140° and 90°W of approximately −0.05°C (results not shown). To isolate the ocean's response to the anticyclonic wind stress in the WPWP, we forced the ocean model with all wind stress anomalies east of the date line removed. The ocean model's response to this wind forcing is a small El Niño with maximum SST anomalies in the eastern equatorial Pacific of approximately 0.2°C (results not shown). Therefore, the anticyclonic anomalies provide a positive feedback, while the easterlies alone provide a negative feedback. These ocean-alone model runs demonstrate that the El Niño in Fig. 13b is due to both the anomalous anticyclonic wind stress in the WPWP and the enhanced westerlies in the central equatorial Pacific.

Figure 14a shows the equatorial SST anomalies from the ocean-only model run forced by winds from the PERT1 model run without SST anomalies in the WPWP over a 4-yr period. Figure 14b shows the change in the equatorial SST anomalies when winds due to the SST anomalies in the WPWP are included. Figure 14b shows that the atmospheric forcing due to the cold SST anomalies in the WPWP causes the SST anomalies in the equatorial eastern Pacific to increase by 10% (when PERT3 winds are used the anomalies are greater than 20%). Comparing the SST anomalies in the central to eastern equatorial Pacific throughout the forced cycle, it is clear that the additional SST anomalies (Fig. 14b) generated by the additional winds (Fig. 12b) tend to enhance and prolong the warm phase of ENSO cycle. The SST budget indicates that both zonal and vertical advection contribute to the additional positive SST anomalies in the central to eastern equatorial Pacific.

Figure 15a shows the equatorial thermocline depth anomalies from the ocean-only model run forced by

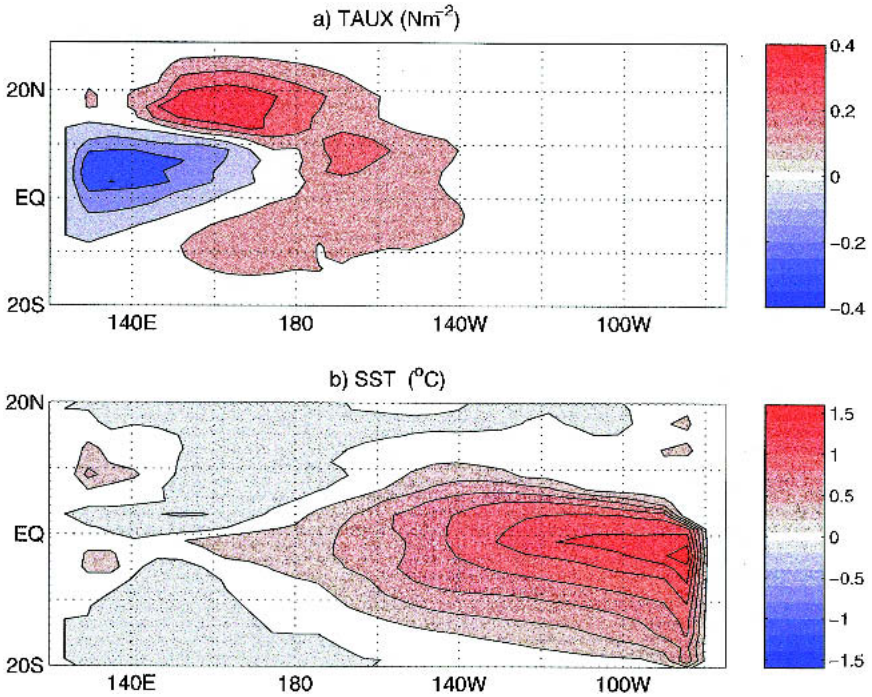

FIG. 13. The ZC ocean model's response to wind stress forced by the cold SST anomalies in the WPWP at the peak of an El Niño event: Model setup described in the text. (a) Zonal wind stress used to force the ocean model, in N m^{-2}. (b) The SST response to this wind stress forcing, in °C.

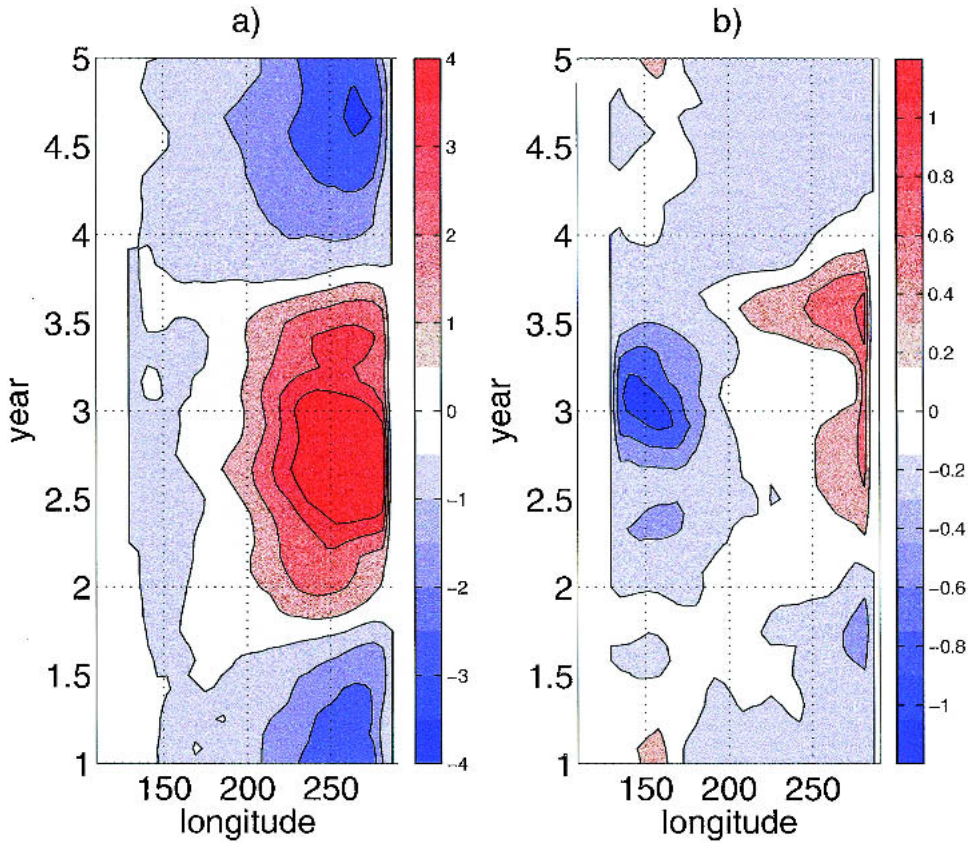

FIG. 14. Equatorial SST anomalies from the stand-alone ZC ocean model runs, in °C: Model setup described in the text. (a) From the model run without forcing from WPWP SSTs. (b) Difference between model runs with and without forcing from WPWP SSTs (with − without).

winds from the PERT1 model run without SST anomalies in the WPWP over a 4-yr period. Figure 15b shows the change in the equatorial thermocline depth anomalies when winds due to the SST anomalies in the WPWP are included. The equatorial zonal wind stress anomalies in the WPWP region only create a very local thermocline tilt change near the edge of warm pool. In this region, it is not the thermocline depth but the zonal currents that are essential for generating SST anomalies. Thus, this local thermocline variability does not play any significant role in generating the SST anomalies shown in Figure 14b. This confirms that the forced oceanic Kelvin wave responses in the equatorial thermocline field to the equatorial western Pacific winds associated with cold SST anomalies in WPWP region largely cancel because of the opposing winds in the central to eastern Pacific. Moreover, one observes a significant increase in the zonal-mean thermocline depth (Fig. 15b) during and even slightly after the ENSO warm phase. According to the recharge oscillator theory, the zonal mean thermocline is about 90° out of phase with the SST in the central to eastern equatorial Pacific (Jin 1997). This can be inferred from Fig. 15a in which the zonal mean thermocline is positive (negative) at the warm to cold (cold to warm) phase transition. The fact that the additional equatorial thermocline anomalies shown in Fig. 15b are largely in the zonal mean and in phase with the SST anomalies in the eastern Pacific implies that there is a significant slowdown of discharge of the equatorial thermocline during the warm phase of ENSO. Thus, the wind stress anomaly and its curl associated with the cold SST anomalies in the WPWP region can enhance ENSO by recharging the equatorial heat content or deepening the equatorial zonal mean thermocline. This enhancement of the warm SSTs also occurs at a later stage in the warm phase of ENSO, as seen in Fig. 14b. Thus, the feedbacks indeed act to prolong ENSO as well.

5. Summary and discussion

In this paper we have explored the impact of ocean–atmosphere feedbacks in the WPWP on ENSO cycles using observations and an intermediate coupled ocean–atmosphere model of the tropical Pacific. Our observational analysis clearly showed that different processes are responsible for forcing cold SST anomalies during

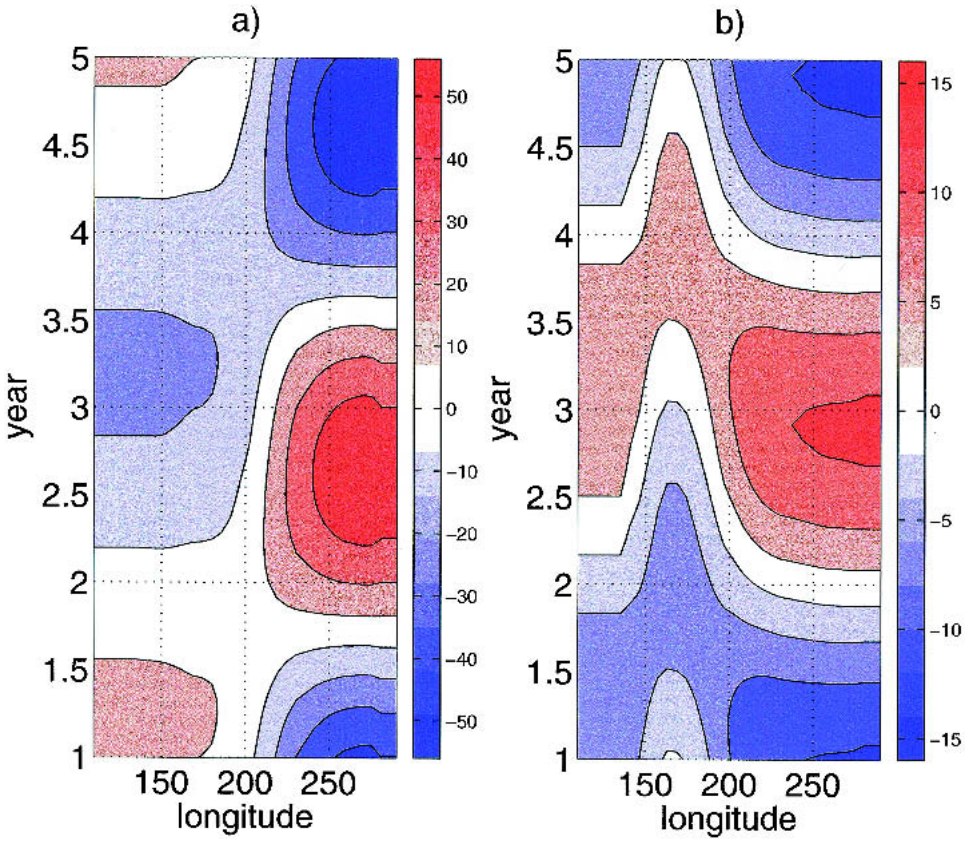

FIG. 15. As in Fig. 14 but for equatorial thermocline depth anomalies, in m.

El Niño events in the Niño-6N and Niño-6S regions. It was found that anomalies in the Niño-6S region form due to three-dimensional subsurface processes, while anomalies in the Niño-6N region form due to surface fluxes. It was also shown that SST anomalies in the Niño-6S region peak before and during an ENSO event, while anomalies in the Niño-6N region peak after a peak in the Niño-3.4 region. An analysis of upper-ocean temperature and surface heat flux anomalies demonstrated that the thermocline comes close to the surface where diurnal processes can mix the cold thermocline water into the mixed layer generating SST anomalies of the order of 1°C.

A crude approximation of ocean mixing processes was then added to the Zebiak and Cane intermediate coupled model of the tropical Pacific by parameterizing the diurnal mixing of thermocline water into the mixed layer when the thermocline becomes shallow as a diffusion with a time scale between 150 and 300 days. It was found that allowing for a dynamic feedback loop in the western Pacific caused the interannual variability of the model to become stronger and more regular.

Model runs with the atmospheric part of the ZC model alone showed that the atmospheric response to cold SST anomalies in the WPWP region consists of not only easterly wind anomalies in the equatorial western Pacific but also a broad weaker westerly component in the central Pacific. These equatorial easterly and westerly wind anomalies are parts of the typical asymmetric Gill-type (Gill 1980) response. The equatorial zonal wind anomalies tend to cancel when zonally integrated. The weak equatorial westerly wind anomalies directly enhance the warm SST anomalies in the central to eastern Pacific by reduced upwelling and anomalous warm zonal advection. Further, the uncoupled ZC ocean model runs confirm that the wind stress anomaly and its curl associated with the cold SST anomalies in the WPWP during the warm phase of ENSO effectively reduce the discharge of the equatorial zonal-mean heat content, leading to anomalous deepening of the zonal-mean thermocline depth, enhancing the eastern Pacific warming and delaying the phase transition of the El Niño event (Jin 1997). We would like to stress here that this current study addresses *only* the role of wind stress anomalies forced directly by SST anomalies in the off-equatorial WPWP. In terms of other studies that have been done showing the significance of wind-forced upwelling Kelvin waves at the peak of an El Niño event, our study shows that, in the case of wind stress anomalies forced by SST anomalies in the off-equatorial WPWP, these Kelvin waves are only part of the ocean's response to the anomalous wind forcing and that the

total response needs to be considered to understand the impact of these winds on ENSO cycles.

Our finding about the potential role of cold SST anomalies in the WPWP region on ENSO cycles can be summarized in the schematic Fig. 16. During the mature phase of an El Niño event, background diurnal mixing carries cold subsurface water from the shoaling equatorial thermocline in the northwestern tropical Pacific to the surface layer, generating cold SST anomalies that reach a peak magnitude a few months after the warming in the eastern equatorial Pacific. These cold SST anomalies suppress convection and generate an asymmetrical Gill-type response with anticyclonic wind stress at and to the west of the cold SST anomalies, due to forced atmospheric Rossby waves, and a remote equatorial response to its east, due to the atmospheric Kelvin wave response. The easterly and westerly wind anomalies at the equator tend to cancel when zonally integrated, preventing the winds from altering SST through changes in the thermocline tilt. However, the westerly winds in the central Pacific tend to enhance the warming in the eastern Pacific and prolong the El Niño event. The deepening of the zonal-mean thermocline depth, due to anomalous recharge by the anticyclonic wind stress curl, tends to slow down the discharge process and prolong the El Niño event. In addition, we demonstrate that, if SST anomalies in the WPWP form closer to the equator, the equatorial response is greater, suggesting that anomalies in the Niño-6S region will have a larger impact on ENSO cycles than anomalies that form in the Niño-6N region. Together, these results indicate that the coupled processes in the WPWP region can have a significant impact on ENSO cycles, both in terms of instability and periodicity.

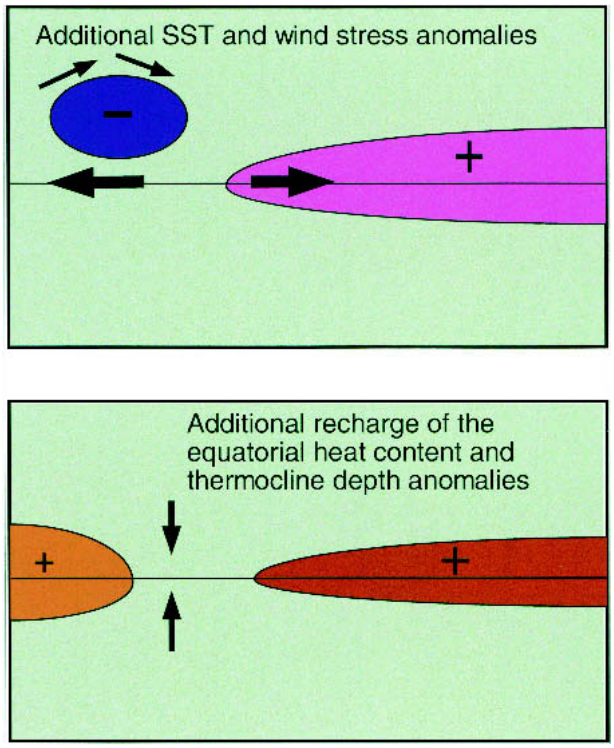

FIG. 16. Schematic of the impact of WPWP cold SSTs on ENSO cycles. (a) The atmospheric response to cold SSTs in the off-equatorial WPWP is composed of both easterlies in the far western equatorial Pacific and westerlies in the central equatorial Pacific (direction of winds shown in bold arrows). The westerlies directly increase the amplitude of the El Niño event. (b) The winds in (a) increase the recharge of equatorial heat content at, and just after, the peak of an El Niño event (direction of recharge/discharge shown in bold arrows).

This new picture about the role of cold SST anomalies equatorward of 12°N in the WPWP region takes into account two important elements of the atmospheric response to the cold SST anomalies in the WPWP region; the broad equatorial westerly response, as the result of the forced atmospheric Kelvin wave response to the east of the asymmetric forcing and the anticyclonic wind stress curl, which tends to recharge the equatorial ocean heat content or increase the zonal-mean thermocline depth (Jin 1997). Our study has demonstrated that, if the total atmospheric response to the cold SST anomalies that form equatorward of 12°N in the WPWP region is considered, the net effect is to enhance and prolong ENSO. However, the possibility that SST anomalies in the WPWP can enhance ENSO cycles needs to be further studied. This requires a better understanding of the oceanic processes in the WPWP region, as well as the role of SST anomalies that form in regions such as the Indian Ocean.

Acknowledgments. FFJ was partly supported by NSF Grants ATM-9615952 and 0226141 and NOAA Grants GC99234 and GC01246. We would like to thank Mike Alexander and an anonymous reviewer for helpful suggestions.

REFERENCES

Battisti, D. S., and A. C. Hirst, 1989: Interannual variability in a tropical atmosphere–ocean model: Influence of the basic state, ocean geometry and nonlinearity. *J. Atmos. Sci.,* **46,** 1687–1712.

Behringer, D. W., M. Ji, and A. Leetmaa, 1998: An improved coupled model for ENSO prediction and implications for ocean initialization. Part I: The ocean data assimilation system. *Mon. Wea. Rev.,* **126,** 1013–1021.

Bjerknes, J., 1969: Atmospheric teleconnections from the equatorial Pacific. *Mon. Wea. Rev.,* **97,** 163–172.

Boulanger, J.-P., and C. Menkes, 1995: Propagation and reflection of long equatorial waves in the Pacific Ocean during the 1992–1993 El Niño. *J. Geophys. Res.,* **100,** 25 041–25 059.

——, and ——, 2001: The TRIDENT Pacific model: II. The thermodynamical model and the role of long equatorial wave reflection during the 1993–1998 TOPEX/POSEIDON period. *Climate Dyn.,* **17,** 175–186.

——, S. Cravatte, and C. Menkes, 2003: Reflected and locally wind-forced interannual equatorial Kelvin waves in the western Pacific Ocean. *J. Geophys. Res.,* **108,** 3311, doi:10.1029/2002JC001760.

Cane, M. A., M. Matthias, and S. E. Zebiak, 1990: A study of

self-excited oscillations of the tropical ocean–atmosphere system. Part I: Linear analysis. *J. Atmos. Sci.,* **47,** 1562–1577.

Carton, J. A., G. Chepurin, X. Cao, and B. S. Giese, 2000a: A Simple Ocean Data Assimilation analysis of the global upper ocean 1950–95. Part I: Methodology. *J. Phys. Oceanogr.,* **30,** 294–309.

——, ——, ——, and ——, 2000b: A simple ocean data assimilation analysis of the global upper ocean 1950–95. Part II: Results. *J. Phys. Oceanogr.,* **30,** 311–326.

Cronin, M. F., and M. J. McPhaden, 1997: The upper ocean heat balance in the western equatorial Pacific warm pool during September–December 1992. *J. Geophys. Res.,* **102,** 8533–8553.

Delcroix, T., J.-P. Boulanger, F. Masia, and C. Menkes, 1994: Geosat-derived sea level and surface current anomalies in the equatorial Pacific, during the 1986–1989 El Niño and La Niña. *J. Geophys. Res.,* **99,** 25 093–25 125.

——, B. Dewitte, Y. du Penhoat, F. Masia, and J. Picaut, 2000: Equatorial waves and warm pool displacements during 1992–1997 ENSO events. *J. Geophys. Res.,* **105,** 26 045–26 062.

Feng, M., P. Hacker, and R. Lukas, 1998: Upper ocean heat and salt balances in response to a westerly wind burst in the western equatorial Pacific during TOGA COARE. *J. Geophys. Res.,* **103,** 10 289–10 311.

Gill, A. E., 1980: Some simple solutions for heat-induced tropical circulation. *Quart. J. Roy. Meteor. Soc.,* **106,** 447–462.

Graham, N. E., and W. B. White, 1988: The El Niño cycle: A natural oscillator of the Pacific ocean–atmosphere system. *Science,* **240,** 1293–1302.

Harrison, D. E., 1996: Vertical velocity variability in the tropical Pacific—A circulation model perspective for JGOFS. *Deep-Sea Res.,* **43B,** 687–705.

Helber, R. W., and R. H. Weisberg, 2001: Equatorial upwelling in the western Pacific warm pool. *J. Geophys. Res.,* **106,** 8989–9003.

Jin, F.-F., 1997: An equatorial ocean recharge paradigm for ENSO. Part I: Conceptual model. *J. Atmos. Sci.,* **54,** 811–829.

Lau, N.-C., and M. J. Nath, 2003: Atmosphere–ocean variations in the Indo–Pacific sector during ENSO episodes. *J. Climate,* **16,** 3–20.

Mangum, L. J., D. C. McClurg, L. D. Stratton, N. N. Soreide, and M. J. McPhaden, 1998: The Tropical Atmosphere Ocean (TAO) Array World Wide Web site. *Argos Newsl.,* **53,** 9–11.

McPhaden, M. J., and X. Yu, 1999: Equatorial waves and the 1997–1998 El Niño. *Geophys. Res. Lett.,* **26,** 2961–2964.

Picaut, J., E. Hackert, A. J. Busalacchi, R. Murtugudde, and G. S. E. Lagerloef, 2002: Mechanisms of the 1997–1998 El Niño–La Niña, as inferred from space-based observations. *J. Geophys. Res.,* **107,** 3037, doi:10.1029/2001JC000850.

Rasmussen, E. M., and T. H. Carpenter, 1982: Variations in tropical sea surface temperature and surface wind fields associated with the Southern Oscillation/El Niño. *Mon. Wea. Rev.,* **110,** 354–384.

Suarez, M. J., and P. S. Schopf, 1988: A delayed action oscillator for ENSO. *J. Atmos. Sci.,* **45,** 3283–3287.

Vialard, J., C. Menkes, J.-P. Boulanger, P. Delecluse, E. Guilyardi, M. J. McPhaden, and G. Madec, 2001: A model study of oceanic mechanisms affecting equatorial Pacific sea surface temperature during the 1997–98 El Niño. *J. Phys. Oceanogr.,* **31,** 1649–1675.

Wang, B., R. Wu, and R. Lukas, 1999: Roles of the western North Pacific wind variation in thermocline adjustment and ENSO phase transition. *J. Meteor. Soc. Japan,* **77,** 1–16.

——, ——, and ——, 2000: Annual adjustment of thermocline in the tropical Pacific Ocean. *J. Climate,* **13,** 596–616.

Wang, C., 2001: A unified oscillator model for the El Niño–Southern Oscillation. *J. Climate,* **14,** 98–115.

——, R. H. Weisberg, and J. I. Virmani, 1999: Western Pacific interannual variability associated with the El Niño–Southern Oscillation. *J. Geophys. Res.,* **104,** 5131–5149.

Weisberg, R. H., and C. Wang, 1997: A western Pacific oscillator paradigm for the El Niño–Southern Oscillation. *Geophys. Res. Lett.,* **24,** 779–782.

Zebiak, S. E., and M. A. Cane, 1987: A model El Niño–Southern Oscillation. *Mon. Wea. Rev.,* **115,** 2262–2278.